Journal of Interfaces, Thin films, and Low dimensional systems 4 (1) Summer and Autumn (2020) 311-322

The effect of hydrostatic pressure on the radiative recombination rate of InGaN/GaN multiple quantum well solar cells

Scientific research paper

Rajab Yahyazadeh*, Zahra Hashempour

Department of Physics, Khoy Branch, Islamic Azad University, Khoy, Iran

ARTICLE INFO

Article history:
Received 3 May 2021
Revised 28 May 2021
Accepted 5 August 2021
Available online 22 October 2021

Keywords:
Recombination rate
Solar cell
Optical absorption
Multi-quantum well

ABSTRACT

In this paper, a numerical model is used to analyze photovoltaic parameters according to the electronic properties of InGaN/GaN multiple-quantum-well solar cells (MQWSC) under hydrostatic pressure. Finite difference techniques have been used to acquire energy eigenvalues and corresponding eigenfunctions of InGaN/GaN MQWSC, where all eigenstates are calculated via a 6×6 k.p method under an applied hydrostatic pressure. All symmetry-allowed transitions up to the fifth subband of the quantum wells (multi-subband model) with barrier optical absorption are considered. The linewidth due to the carrier-carrier and carrier-longitudinal optical (LO) phonon scattering are also considered. A change in pressure up to 10 GPa increases the intraband scattering time up to 38 fs for heavy holes and 40 fs for light holes. The raise in the height of the Lorentz function reduces the excitonic binding energy and decreases the radiative recombination rate up to $0.95\times10^{25}\mathrm{cm}^{-3}\mathrm{s}^{-1}$. The multi-subband model has a positive effect on the radiative recombination rate.

1 Introduction

Recently, indium gallium nitride alloys have attracted much attention for optoelectronic applications [1–4] due to their tunable energy bandgap varying from 0.7 eV to 3.4 eV [5-6]. The absorption range covers a significant portion of the solar spectrum, making InGaN a promising candidate for multi-junction solar cell systems. Moreover, with high radiation resistance, thermal stability, and chemical tolerance, InGaN solar cells could operate in extreme conditions [7]. The temperature and polarization dependence are considered preeminent tools in evaluating optical and electronic characteristics in III-V nanodevices (e.g., solar cells and transistors) [8,9]. The optical absorption coefficients are one of the significant parameters in calculating the recombination rate in InGaN/GaN Multi-quantum solar cell. Therefore, to study the recombination rate in detail, we must calculate the absorption coefficients in InGaN/GaN MQWSC. The effect of alloy on InGaN/GaN MQWSC has been investigated by Deng et al. [10]. Also, the temperature effect on InGaN/GaN MQWSC has been studied by Belghouthi et al. [11] where its efficiency in different wells and temperatures has been considered by Chouchen et al. [12]. In all these studies, a simple analytical relation of quantum well absorption coefficient has been used to obtain the electrical and electronic characteristics; however, the role of quantum barrier absorption coefficient has still not been taken into account. Also, in our previous work [13], the absorption coefficient of quantum wells has been

*Corresponding author.
Email address: Rajab.yahyazadeh@iaukhoy.ac.ir
DOI: 10.22051/jitl.2021.35972.1053

calculated for the first subband transition without considering other subbands. We had not considered the effect of barrier optical absorption, three-dimensional exciton binding energy, and the linewidth due to the carrier-carrier and carrier-longitudinal optical (LO) phonon scattering under external disturbances. This paper aims to perform these corrections under an external perturbation (e.g., hydrostatic pressure). In solar cells with a single-quantum well in the intrinsic region, due to the low absorption coefficient of second- and higher-order subbands, these energy transitions are not very effective in the recombination rate; however, in multi-quantum wells in the intrinsic region, the second-and higher-order transitions significantly affect the recombination rate due to more quantum wells. The linewidth function (Lorentz function) is one of the most important functions for calculating optical parameters, such as optical absorption coefficient and gain. The optical absorption coefficient is one of the significant parameters in calculating photocurrent density in the InGaN/GaN Multi-quantum solar cell. The Lorentz function also depends on the scattering time and the transition energies. In all the work done on solar cells, this transition time under external perturbations is fixed and often considered to be 0.1ps; in the present study, we examine its dependence on pressure. The most important advantage of this numerical method and the aspect of innovation in this work is the use of five important parameters, including effective mass, energy gap, lattice constants, dielectric constant and quantum barrier, and well thickness, all of which are simultaneously dependent on hydrostatic pressure and temperature. We also consider the effect of hydrostatic pressure on the energy of heavy and light holes and the transition energy of the subbands. In this model, the conduction band energy, wave functions, and energy subbands are obtained from the self-consistent solution of the Schrodinger and Poisson equations. The hole valance bands (heavy and light hole) energy, wave functions, and energy subbands are calculated using a 6×6 k.p method. The sample used in the modelling is the p–i–n solar cells with an InGaN/GaN MQWSC structure within the i-region. The p and n regions are based on GaN. The donor and acceptor concentrations in the n- and p-region materials are assumed to be equal to $0.1\times10^{18}cm^{-3}$, and 10 wells are considered in the present work. It should be notified that the calculated built-in polarization field for the structures is about $\sim10^{8}Vm^{-1}$. In the present study, atmospheric and hydrostatic pressures are taken into account, i.e., at zero hydrostatic pressure only the atmospheric pressure is applied. The results and discussions are obtained by calculating and drawing the figures.

2 Calculation Model

2.1 Self-consistent solution of Schrödinger-Poisson equations

The quantum well solar cell (QWSC) consists of a multiple quantum well structure in the intrinsic region of a p–i–n. The MQW structure introduced for the model is constructed by $In_mGa_{1-m}N$ with lower indium molar fraction (m=0.5) for wells and m=0.4 for barriers, as shown in Fig. 1. To obtain accurate values for Fermi energy, the energies of quantized levels within the two-dimensional electron gas (2DEG), potential profiles, wave function, and the sheet carrier concentration for the 2DEG in InGaN/GaN heterostructures for both Schrodinger and Poisson equations must be solved. This is achieved by solving Schrodinger's equation and simultaneously taking into account the electrostatic potential obtained from Poisson's equation, as well as the image and exchange-correlation potentials using the three-point finite difference method [14]. In the Schrodinger equation, eF_zz is the potential energy induced by the polarization charges, F_z is the electric fields in the well, F_w, and barrier, F_b, caused by the spontaneous (SP) and piezoelectric (PZ) polarization [15-17]. In this work, five parameters, including effective mass, energy gap, lattice constants, dielectric constant and quantum barrier, and well thickness are used which are simultaneously dependent on the hydrostatic pressure and temperature as follows:

1- The basal strain represented as of the form $\grave{o}(T,P,m)=\left(a_s-a_e(T,P,m)\right)/a_e(T,P,m)$ is expressed from the lattice of the substrate a_z and the epilayer $a_e(T,P,m)=a_0(m)\left[\left(1+\beta\left(T-T_{ref}\right)\right)\left(1-P/3B_0\right)\right]$. The lattice constants, as a function of temperature, indium molar fraction and the hydrostatic pressure [18-20], where $B_0=239GPa$ is the bulk modulus of sapphire, $\beta_{GaN}=5.56\times10^{-6}K^{-1}$ is the thermal expansion coefficient at $T_{ref}=300K$, $a_0(m)=0.13989m+0.03862$ is the equilibrium lattice constant as a function of the indium molar fraction [19,20].

2- Here $\mathcal{E}_{GaN}(T,P)$ and $\mathcal{E}_{InGaN}(m,T,P)$ are the dielectric constants of GaN and InGaN while $L_{In_mGa_{1-m}N}(T,P)$ and L_{GaN} are respectively the thickness of InGaN and GaN as given by [20]:

$$\varepsilon_{GaN}(T,P)=10\times\exp\left(10^{-4}\left(T-T_0\right)-6.7\times10^{-3}P\right) \quad (1)$$

$$\varepsilon_{InGaN}(m,T,P)=\varepsilon^{GaN}(T,P)+6.4m \quad , \quad (2)$$

$$L_b = L_{In_mGa_{1-m}N}(T,P) = L_{InGaN}(0)\left[-\left(S_{11}^{In_mGa_{1-m}N} + 2S_{12}^{In_mGa_{1-m}N}\right)P\right], \quad (3)$$

$$L_w = L_{GaN}(T,P) = L_{GaN}(0)\left[-\left(S_{11}^{GaN} + 2S_{12}^{GaN}\right)P\right] \quad . \quad (4)$$

Here, $L_{InGaN}(0)$ and $L_{GaN}(0)$ are the InGaN and GaN layers thickness without hydrostatic pressure and temperature. S_{11} and S_{12} are the elastic compliance constants.

3-The band gap energy of InGaN/GaN is as follows [15, 18, and 20]:

$$E_g(T,P) = E_g(0,0) + \gamma P + \sigma P^2 + \left(\alpha T^2\right)/(T + T_e) \quad , \quad (5)$$

where $E_g(0,0)$ stands for the band gap energy of GaN or InGaN in the absence of the hydrostatic pressure at temperature 0K. The suggested parameters used in Eq. (5) have been taken from Ref 24. In this work the parameters α, σ, γ etc. are independent of the electron concentration.

4-In the Schrödinger equation the electron effective mass m^* can be written as [21]:

$$\frac{m_0}{m_e^*(P,T,m)} = 1 + \frac{E_P^\Gamma\left(E_g^\Gamma(P,T,m) + 2\Delta_{S0}/3\right)}{E_g^\Gamma\left(E_g^\Gamma(P,T,m) + \Delta_{S0}\right)} \quad , \quad (6)$$

where m_0 is the free electron mass, E_P is the energy linked to the momentum matrix element, Δ_{S0} is the spin-orbit splitting, and $E_g^\Gamma(P,T,m)$ is the band gap variation as a function of the hydrostatic pressure and temperature. The whole wave functions and energy subbands are calculated along the z-axis using a $\times 6$ k.p method [22,23].

The optical absorption expression as a function of the photon energy E' is calculated as [24,25]:

$$\alpha_W(E') = \frac{\pi\hbar q^2}{E'\varepsilon_0 m_0^2 c n_{eff}} \times \sum_{i,j}^{n} \int_{E_{g,w}}^{g,b} D_{r,ij}^{2D} |Mij|^2 \left(f_{i_v} - f_{j_c}\right) L\left(E' - E_{ij}\right) dE_{ij}, \quad (7)$$

where q and c are respectively the electron charge and light vacuum speed; i and j are respectively the conduction and valance subband number.

$L\left(E' - E_{ij}\right) = \left(\Gamma_{hom}^2\right)/2\pi\left[\left(E' - E_{ij}\right)^2 + \Gamma_{hom}^2\right]$ is the Lorentzian function, $D_r^{2D} = m_{r,ij}/\left(\pi\hbar^2 W\right)$ is the reduced density of the allowed transition of each subband while $|M_{ij}|$ represents the transition strengths. These three parameters are important in optical absorption. The Lorentz function depends on parameters Γ_{hom} and E_{ii}, where Γ_{hom} represents the linewidth of the conduction and the valance bands that is related to scattering of all carriers (electrons, light, and heavy holes) and phonons (see Appendix A) [26,27]. The intraband relaxation time τ_{in} is obtained from Eqs. (A1) and (A4) as $\hbar/\tau_{in} = \Gamma_{cjk_\square}(E) + \Gamma_{vjk_\square}(E)$. Another effective parameter regarding the Lorentz function is $E_{ij} = E_i^e + E_j^h + E_g^{GaN} - E_b^{ij} - eF_W L_W$ [28]. That is the transition energy of the electron from the conduction band to the valance band, where E_i and E_j are respectively the subband energy of the electron and holes in the triangular quantum well while E_b is the bounding energy of excitons which is dependent on external perturbations such as pressure and temperature through electron and hole effective masses [28-30]. Exciton energies are determined by employing a variational procedure [31]. Restricting ourselves to the analysis of s-like excitons implies the proposal of a normalized trial wavefunction, $|\Psi_x\rangle$, built from the product of uncorrelated electron and hole subband states together with the inclusion of a hydrogenic-s-like factor [32-34]. Then, the exciton energy is obtained by minimizing the functional $E_x = \langle\Psi_x|H_x|\Psi_x\rangle/\langle\Psi_x|\Psi_x\rangle$ where $H_x = H_e + H_{hh,lh} + H_\perp$ is the exciton Hamiltonian that includes the electron one-band Hamiltonian from the Schrodinger equation (H_e), the heavy and light hole six-band Hamiltonian from the K.P model $(H_{hh,lh})$, and the electron-hole interaction Hamiltonian $(H_\perp)$ [31-34]. The binding energy of the s-like exciton resulting from the coupling of the electron in the i-th subband and the hole in the j-th subband is then given by $E_b^{ij} = E_i^e + E_j^h - E_x$ [31]. The carrier effective mass in the i-th sub band can be calculated as follows [35,26]

$$\frac{1}{m_i^*} = \frac{1}{m_b^*}\left[1 - P_{iw}\right] + \frac{1}{m_w^*}P_{iw} \quad , \quad (8)$$

where m_b^* and m_w^* are the barrier and well carrier effective masses, $P_{iw} = P_{iw}(\psi_{iw})/\left(P_{ib}(\psi_{ib}) + P_{iw}(\psi_{iw})\right)$ is the probability of finding an electron in the quantum

well at the level with energy E_i. $P_{iw}(\psi_{iw}) = \int_0^{d_{GaN}} dz|\psi_{iw}|^2$ and $P_{ib}(\psi_{ib}) = \int_{-d_{InGaN}}^{0} dz|\psi_{ib}|^2$ respectively represent the wave function of the electron in the i-th subband and the wave function penetrating towards the quantum barrier. The value of the penetrating wave function in the barrier $(P_{ib}(\psi_{ib}))$, is the criterion for calculating the quantum confinement that is effective on the effective masses of the carriers in subbands. The effective masses of light and heavy holes are obtained using the $\times 6$ k.p method [36]. The numerical values of the valance band effective mass parameters (Ai) and deformation potentials (Di) are taken from reference [21]. By determining the effective masses of carriers in quantum wells, through ternary formula $1/m^*_{In_xGa_{1-x}N} = \left((1-x)/m^*_{InN}\right) + x/m^*_{GaN}$, the effective masses in $m^*_{In_xGa_{1-x}N}$ barriers can be obtained [37]. By determining the effective mass of the electron in the i-th conduction subband and the effective mass of the hole in the j-th valance subband, the reduced effective mass $m^{*-1}_{r,ij} = m_i^{-1} + m_j^{-1}$ can be calculated. As a result, the reduced density of the allowed transition can be calculated where W is the thickness of quantum well. The transition matrix element $|M|^{\angle}$ is a measure for the strength of stimulated electron transitions in a given material. This strength does not depend on the direction of the intraband transition; it is the same for emission and absorption. However, the transition strength does depend on the angle between the electron wave vector $\vec{k}$ and the optical field vector $\vec{E}$. Any polarization direction of the optical field encounters a variety of electron $\vec{k}$ vectors that needs to be averaged at the given photon energy. For bulk zinc blende semiconductors, averaging over all possible $\vec{k}$ vectors results in an isotropic transition matrix element that is equal to the momentum matrix element given by $M_b = (m_0 E_p)/6$ [25]. E_p, is the energy parameter whose numerical value is given in Table One. For quantum well structures, the transition matrix element is anisotropic while the absorption coefficient depends on the optical polarization. Commonly, one distinguishes two polarization modes, in which either the electric field (TE mode) or the magnetic field (TM mode) lies within the quantum well *xy*-plane (transversal plane). The compression strain increases the mean band gap and splits the degeneracy of the valence band maximum and introduces an anisotropic valence band structure. Note that the highest band is now heavy along, $k_\perp$, the strain axis (growth direction) with light holes along $k_\parallel$. Consequently, the light beam has TE mode. The transition strengths of the TE mode are different for heavy (hh) and light holes (lh) Which are calculated as [25, 38]

$$\left|M^{TE}_{e-hh}\right|^2 = \left(3+3\cos^2(\theta_e)\right)C_{ij}\left|M_b^2\right|/4, \quad (9)$$

$$\left|M^{TE}_{e-lh}\right|^2 = \left(5-3\cos^2(\theta_e)\right)C_{ij}\left|M_b^2\right|/4, \quad (10)$$

where $\cos(\theta_e) = E_{ij}/E'$ is the angular factor. $C_{ij} = \int \psi_i^*(x)\psi_j(x)dx$ is the electron-hole overlap integral. For the TM mode, the relationships are similar to Eqs. (17) and (18), except that the inside of the parentheses in Eq. (8) is $3-3\cos^2(\theta_e)$ (for heavy holes) and $1+3\cos^2(\theta_e)$ (for light holes). It should be noted that due to the finiteness of the quantum barriers, the orthogonal condition in the overlap integral as well as selection rule (i=j) is no longer imposed as all symmetry-allowed transition are considered. $f_{i_c} = 1/1+\exp\left(E_{i_c} - E_{f_c}\right)/k_bT$ and $f_{j_v} = 1/\left[1+\exp\left[\left(E_{j_v} - E_{f_v}\right)/k_bT\right]\right]$ are the Fermi-Dirac distribution for electrons in the i-th subband of the conduction bands and holes in the j-th subband of valance bands, respectively. E_{i_c} and E_{j_v} are the quantized electron and hole energy levels, respectively. E_{f_c} and E_{f_v} are the electron and hole quasi-Fermi levels, respectively. Finally, Adach's refractive index model for $In_mGa_{1-m}N$ is given by [25]:

$$n_{eff} = \sqrt{A\left(\hbar\omega/E_g\right)^{-2}\left\{2-2\sqrt{1+\left(\hbar\omega/E_g\right)}\right\}+B.} \quad (11)$$

Here $A = 9.827(1-m)-53.57m$ and $B = 2.736(1-m)-9.19m$ are alloy-dependent parameters that are true for $m<0.38$. The absorption coefficient of the quantum barrier for continuous states is as follows [42]:

$$\alpha_B(E') = \frac{e^2|\hat{e}\cdot\underline{p}_{cv}|^2}{n_{eff}c\varepsilon_0 m_0 E' R_y a_0^3} \times \left(\int_{E_g^{In_{0.4}Ga_{0.6}N}}^{\infty} \frac{d\varepsilon'}{1-\exp\left(-2\pi/\sqrt{\varepsilon'}\right)} \frac{\Gamma_{\text{hom}}}{(\varepsilon-\varepsilon')^2+\Gamma^2_{\text{hom}}}\right), \quad (12)$$

where R_y and a_0 are the exciton Rydberg energy and Bohr radius, respectively, $\varepsilon = \left(E'-E_g\right)/R_y$ is the normalized energy measured from the bandgap, and

$\left|\hat{e}.p_{cv}\right|^2 = m_0 E_p/6$ is the momentum-matrix element of the bulk quantum barrier. The radiative recombination rate is given by [43]:

$$U_{rad} = B_{rad}(np - n_i^2)\,. \tag{13}$$

Here n and p are the densities of electrons and holes in the conduction and valance bands, respectively, while n_i is the intrinsic densities of the carriers. The recombination coefficient depends on the absorption coefficient is calculated from the following equation

$$B_{rad} = \frac{2\pi}{n_i^2 h^3 c^2}\int_{E_g^{11}}^{\infty} n_{eff}^2\,\alpha(E)e^{-E/k_B T}E^2 dE\ . \tag{14}$$

If we calculate B_{rad} in a quantum barrier or well, we put their absorption coefficients in Eq. (14). The lower limits of the integral, n_i and n_{eff}, are also functions of the quantum barrier and well areas. The exponential term means that, relative to absorption, the contribution from the energy level closer to the band edge is much more important.

3 Results and Discussion

In this paper, a numerical model is presented to calculate the optical parameters of InGaN/GaN MQW Solar Cells (MQWSC) in order to investigate the effect of hydrostatic pressure. The Schrodinger and Poisson differential equations are solved by the finite difference method. Regarding the self-consistent solution of Schrodinger-Poisson equations, the iterative method mentioned in Refs. [39] and [40] is used. The convergence is obtained when the difference on the Fermi level associated with two consecutive iterations ($E_{F(n)} - E_{F(n-1)}$) is smaller than $10^{-4}eV$; also, during the calculations, the same grid mesh is used for both Poisson and Schrödinger equations. The hole eigenstates are calculated along the z-axis using a $\times 6$ k.p method. Figure 1 shows the dependence of the conduction band offset, the bandgaps of InGaN, and GaN on the hydrostatic pressure. The increase in the hydrostatic pressure with a range of 0-10Pa leads to increased conduction band offset. This is attributed to an increase in the bandgap energy of GaN and InGaN with increased hydrostatic pressure. This phenomenon is related to the correction of the atomic distances of the crystal lattice by external pressure, leading to a change in polarization. Conduction and valance bands with the location of quantum wells (electrons and holes), as well as valance bands for light and heavy holes, are shown in Fig. 2. The optical absorption equation is proportional to the spatial overlap of electron-hole wave functions, $C_{ij,P}$ (P = 0, 5, 10), with 0 corresponding to the device under no pressure. The overlap regarding different pressures relative to $C_{ij,0}$ is extracted and plotted for the first and second subbands in Fig. 3. As can be seen, the increase in the pressure decreases the spatial overlap while it increases the depth of quantum wells. Increased depth of the wells leads to increasing the electron and hole densities while decreasing the propagation of the wave functions (electrons and holes). As a result, the quantum confinement increases and decreases the overlap. The Lorentz function is one of the most influential parameters in the optical absorption equation in addition to its shape. To examine this function in detail, the pressure dependence of the conduction and valance linewidths is calculated, as illustrated in Figs. 4 and 5, respectively. In particular, line widths have a decreasing trend with increasing pressure. This is since the spatial separation of wave functions decreases with increasing carrier density. In the case of scattering carriers with phonons (electron-phonon, heavy hole-phonon, light hole-phonon), the decrease in linewidths is due to decreasing the term related to the Fermi function in the second term in the square bracket of Eq. (A4). The difference between the subband energy and the Fermi energy increases with increasing hydrostatic pressure, resulting in the decrease in the term related to the Fermi function. A reduction in the linewidths of the conduction and the valance bands increases the intraband relaxation time between the electrons and the light and heavy holes, as shown in Fig. 6, due to the inverse relationship of intraband relaxation time with linewidths. According to Fig. 6, an increase in the pressure by 10 GPa changes the relaxation time to a mean of 38fs for heavy holes and 40fs for light holes. These changes are taken into account in the calculation of the Lorentz function. At zero pressure for heavy holes, this value is equal to 0.97 ps, approximately 0.1ps. In the calculations of other studies (mentioned in the introduction) under changes such as barrier width, well width, various barrier alloys, and external perturbation, this value is considered constant and equal to 0.1ps. Transition energy is an effective parameter in calculating the Lorentz function, which also depends on the exciton binding energy and the subbands energy of the quantum wells. To better show the changes in these parameters, the second and third subbands are illustrated; however, in the calculations, symmetric-allowed transitions up to the fifth subband are entered. Of course, it should be noted that the first and second subbands have the greatest effect (due to their high density). The binding energy of excitons as a function of hydrostatic pressure is shown in Fig. 7. As seen Fig. 7, the decrease in the binding energy of excitons dependence with increasing pressure can be explained by the band offset and the internal

electric fields (F_w and F_b). With increasing pressure, the spontaneous and piezoelectric polarization increase, increasing the internal electric fields. The electric fields separate the electron and holes in the opposite direction, which reduces the overlap of electron and hole wave functions (Fig. 3), thus decreasing the binding energy of excitons. As the pressure increases, the band offset increases (Fig. 1), which expands the distance between the electrons and holes, thus reducing the Coulomb interaction. It also increases the depth of quantum wells, electron density, and quantum confinement, thus ultimately reducing the exciton binding energy. By determining the energy of the subbands related to the carriers and the binding energy of excitons, the transition energy of the carriers can be calculated, as shown in Fig. 8. According to the figure, with increasing pressure, the transition energies increase. By determining the transition energies and the linewidths of the carrier, the Lorentz function for light and heavy holes of all symmetry-allowed transitions can be obtained. For example, the Lorentz function of the first subband transition corresponding to light and heavy holes is plotted in Fig. 9. According to Fig. 9, with increasing pressure, the height of the Lorentz function increases while its width decreases. They shift to higher energies as the pressure increases. As the pressure increases to 10, the height of the Lorentz function increases to $27eV^{-1}$ for heavy holes and $16eV^{-1}$ for light holes. This increase, along with the decrease in width, is related to the decrease in linewidths, as illustrated in Figs. 4 and 5. The Lorentz function transfer to high energies is associated with the increase of transition energies with increasing pressure. By determining the Lorentz and the overlap function, as well as other parameters, the well absorption coefficient in terms of wavelength is plotted in Fig. 10. In Fig. 10, the well absorption coefficient of other electronic transitions is also considered. The pressure effect on the absorption coefficient of quantum wells is illustrated. According to Fig. 10, the absorption coefficient decreases by increasing pressure, which is related to the increase in the energy gap. Light holes have more energy gaps than heavy holes; thus, they have less absorption. Consequently, the smaller peak corresponds to a light hole.

Table 1. Suggested parameters for GaN and InN

Parameters(unit)	GaN	InN	References
$\mathbf{E_P^{\Gamma}(eV)}$	14.0	14.5	[21]
$\mathbf{E_g^{\Gamma}(0K=0GPa)(eV)}$	3.42	0.7	[21]
$\mathbf{\Delta_{s0}(eV)}$	0.014	-0.001	[21]
$\boldsymbol{\gamma}\mathbf{(meV.GPa^{-1})}$	31.8	16	[19]
$\boldsymbol{\delta}\mathbf{(meV.GPa^{-2})}$	-0.23	-0.02	[19]
$\mathbf{S_{11}(10^{-2}GPa)}$	0.55	1.15	[16]
$\mathbf{S_{12}(10^{-2}GPa)}$	0.19	0.46	[16]
$\boldsymbol{\alpha}\mathbf{(10^{-3}eV.K^{-1})}$	0.909	0.245	[21]
$\mathbf{T_e(K)}$	830	624	[21]
$\boldsymbol{\varepsilon_{\infty}}$	5.39	6.7	[44]

The absorption coefficient of a bulk quantum barrier in terms of wavelength at different pressures is shown in the inset. In this figure, there are two peaks but very close to each other, which is due to the proximity of the energy levels of the light and heavy holes at the band adage $k_{\|}$ (unlike GaAs degenerated in $k_{\|}$). Also, the absorption coefficient decreases with increasing pressure. The reason is the same as for the decrease in the absorption coefficient of the quantum well and is related to the increase in the energy gap. By determining the absorption coefficients, the recombination coefficients can be calculated, as observed in Fig. 11. In Fig. 11, the recombination coefficients according to Eq. (14) are dependent on the absorption coefficients. Therefore, with increasing pressure, the recombination coefficients decrease as the adsorption coefficients decrease. The main reason for this decrease is related to the increase in the depth of quantum wells and quantum confinement. As the pressure increases to 10 Gpa, the recombination coefficients decrease to $0.5\times10^{10}cm^3s^{-1}$ for quantum wells (B_w) and $0.4\times10^{10}cm^3s^{-1}$ for quantum barriers (B_b). Finally, the radiative recombination rate in terms of the distance at different pressures is illustrated in Fig. 12. In Fig. 12, the radiative recombination rate decreases with increasing pressure, which is also related to the decreasing changes of the recombination coefficient with increasing pressure. As the pressure increases by an order of magnitude, the radiative recombination rate decreases by an average of $0.95\times10^{25}cm^{-3}s^{-1}$.

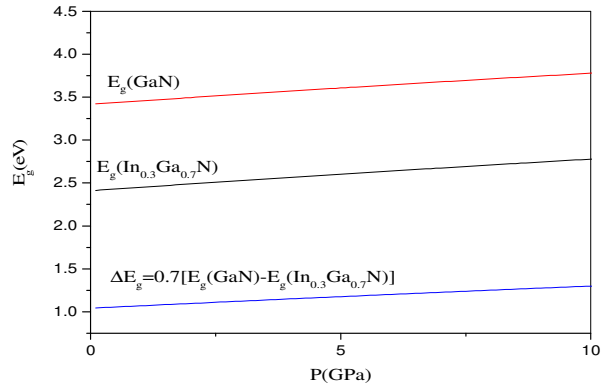

Figure 1. Bandgaps energy of InGaN, GaN, and conduction band offset of InGaN/GaN MQW solar cell as a function of pressure.

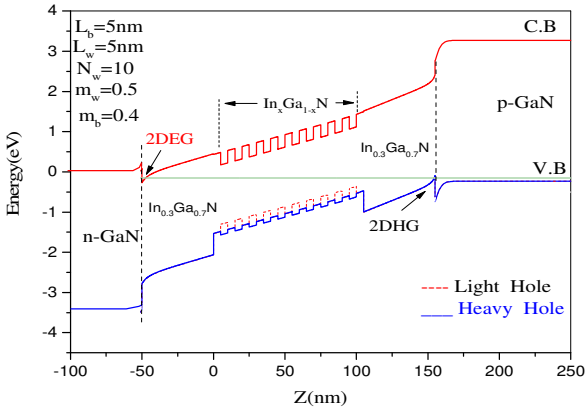

Figure 2. The conduction (C.B) and valance(V.B) bands energy of InGaN/GaN MQW solar cell as a function of the distance under different hydrostatic pressure.

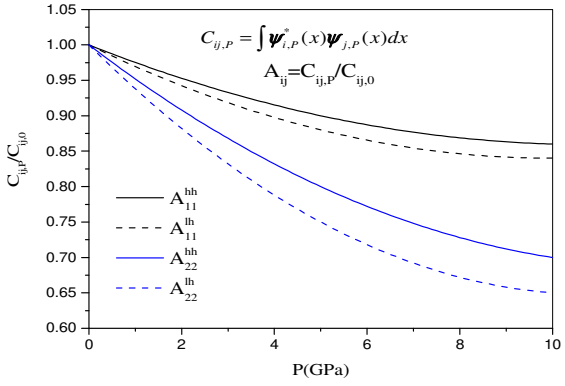

Figure 3. Normalized overlap of the electron–hole wave functions versus hydrostatic pressure. for InGaN/GaN MQW solar cell..

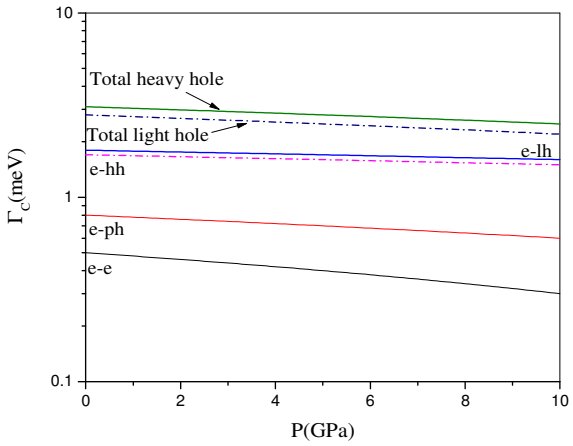

Figure 4. Conduction band linewidths as a function of hydrostatic pressure at subband adage $k_{\parallel}$ for InGaN/GaN MQW solar cell. In which all the scattering of electrons with other electrons (e-e), phonons (e-ph), light holes (e-lh) and heavy hole (e-hh) are considered.

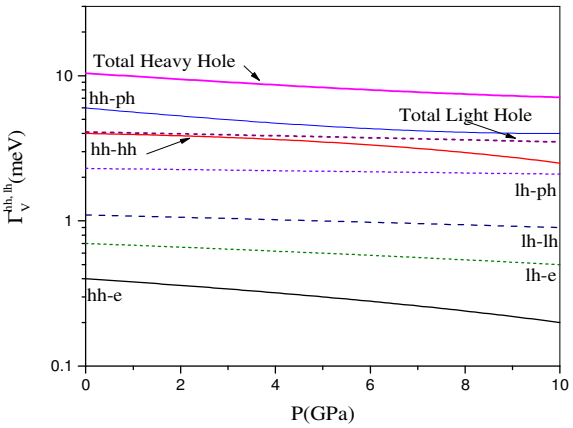

Figure 5. Valance band linewidths as a function of hydrostatic pressure at subband adage $k_{\parallel}$ for InGaN/GaN MQW solar cell. In which all the scattering of holes with other holes (hh-hh, lh-lh), phonons (lh-ph, hh-ph) and with other electrons (e-hh, e-lh) are considered.

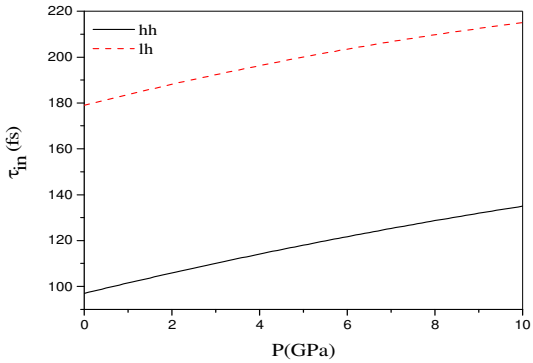

Figure 6. Intraband relaxation time as a function of hydrostatic pressure at subband adage $k_{\|}$ for InGaN/GaN MQW solar cell. In which heavy hole (solid line) and light hole (dashed line) are considered.

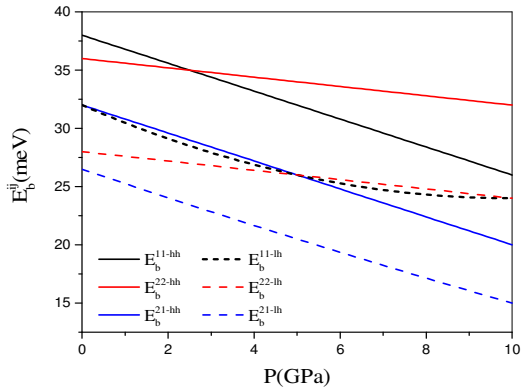

Figure 7. Exciton Binding energy of heavy holes and light holes as a function of hydrostatic pressure for InGaN/GaN MQW solar cells.

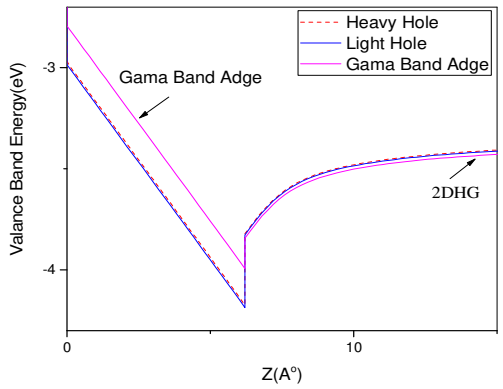

Figure 8. Transition energy as a function of hydrostatic pressure at subband adage $k_{\|}$ for InGaN/GaN MQW solar cell. In which heavy hole (solid line) and light hole (dashed line) are considered.

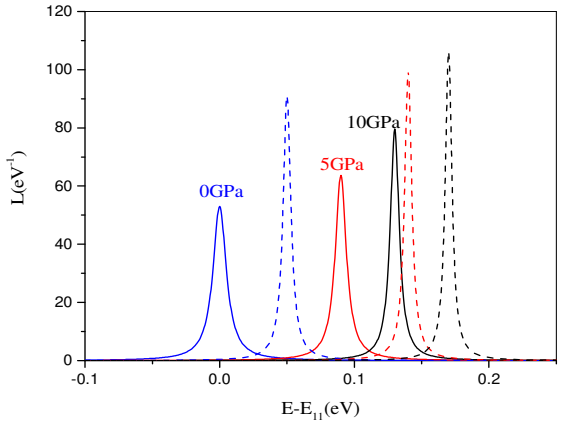

Figure 9. Heavy hole (solid line) and light hole (dashed line) Lorentzian function versus of the energy difference $(E - E_{11})$ under different hydrostatic pressures for InGaN/GaN MQW solar cell, In which the energy transition between the first subbands of electron energy levels with holes are considered.

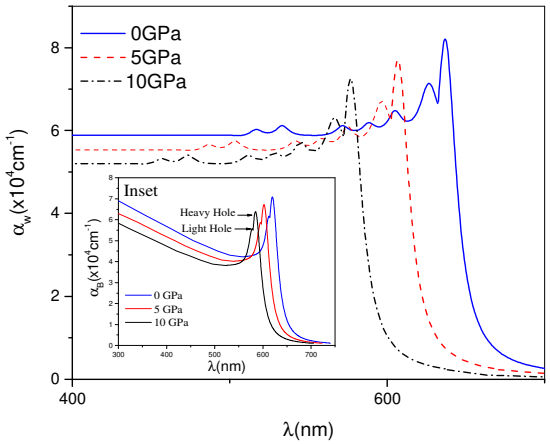

Figure 10. Quantum well optical absorption versus wavelength under different hydrostatic pressures for InGaN/GaN MQW solar cell. Inset: Quantum barrier optical absorption versus wavelength under different hydrostatic pressures for InGaN/GaN MQW solar cell.

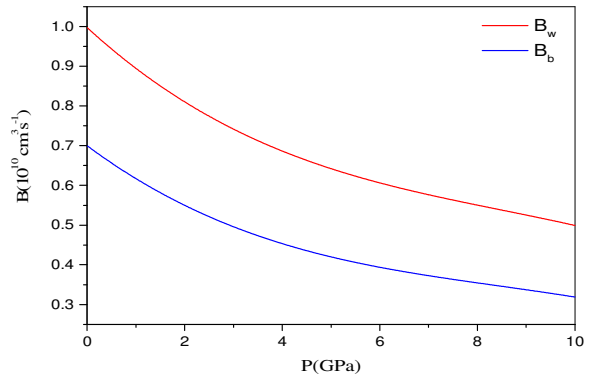

Figure 11. Recombination coefficients versus different hydrostatic pressures for InGaN/GaN MQW solar cell.

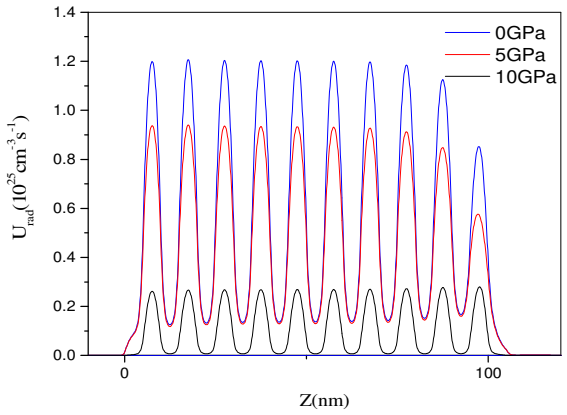

Figure 12. Radiative recombination rate of InGaN/GaN MQW solar cell as a function of the distance under different hydrostatic pressure.

4 Conclusions

In this study, we examined the optical absorption spectrum, absorption coefficient, and radiative recombination rate of InGaN/GaN multi-quantum-well solar cells (MQWSC) under hydrostatic pressure. The results showed that increasing the hydrostatic pressure in the range of 0-10 GPa would lead to an increase in (I) the intraband relaxation time up to 38fs for heavy holes and 40fs for light holes and (II) the height of the Lorentz function to 27eV^{-1} for heavy holes and 17eV^{-1} for light holes, as well as a reduction in (III) the overlap of normalized wave functions and excitonic binding energy (IV) the recombination coefficients to $0.5\times10^{10}\,cm^3s^{-1}$ for quantum wells and $0.4\times10^{10}\,cm^3s^{-1}$ for quantum barriers and (V) the radiative recombination rate up to $9.5\times10^{25}\,cm^{-3}s^{-1}$. Therefore, it can be concluded that all effective transitions of quantum wells should be considered for an accurate study of radiative recombination rate. Also, the absorption coefficient of a bulk quantum barrier is effective in obtaining an accurate radiative recombination rate.

Acknowledgements

The authors would like to thank Khoy Branch (Islamic Azad University) for the financial support of this research, which is based on the research project contract.

Appendix A: Intraband Relaxation Time

The linewidth due to the carrier-carrier scattering is obtained from the perturbation expansion of one-particle Green's functions. The linewidth for carrier-carrier scattering is given by:

$$\begin{aligned}&\Gamma^{c-c}_{njk_\parallel}\\&=\pi\sum_{n'=c,v}\sum_{k',p}\sum_{i,j}\left|V_{nm}(k_\parallel k'_\parallel,ii',jj')\right|\times\delta\big(E\\&+E_{n'ip_\parallel}-E_{nj'k_\parallel}-E_{n'i'p'_\parallel}\big)\\&\times\left[f_n\big(E_{nj'k_\parallel}\big)f_{n'}\big(E_{n'i'p'_\parallel}\big)\{1-f_{n'}\big(E_{n'ip_\parallel}\big)\}\right.\\&+\{1-f_n\big(E_{nj'k'_\parallel}\big)\}\{1\\&\left.-f_{n'}\big(E_{n'ip'_\parallel}\big)\}f_{n'}\big(E_{n'ip_\parallel}\big)\right],\end{aligned}\qquad(A1)$$

where n refers to conduction (n = c) or valence (n = v) bands, i, i', j, and j' are the subband numbers of the QW structure, and $f_n(E)$ is the Fermi distribution function. The interaction matrix element V_{nm} in a two-dimensional QW is given by

$$\begin{aligned}&V_{nm}(k_\parallel k'_\parallel,ii',jj')\\&=\frac{e^2}{2\varepsilon_{GaN}A}\frac{\delta(k_\parallel-k'_\parallel,p'_\parallel-p_\parallel)}{\sqrt{|k_\parallel-k'|+\lambda_s^2}}\\&\times\int\int\phi^*_{nj'}(z_1)\phi_{nj}(z_1)\phi^*_{ni'}(z_2)\phi_{n'i'}(z_1)\\&\times\exp\left(-|z_1-z_2|\sqrt{|k_\parallel-k'|^2+\lambda_s^2}\right)dz_1dz_2,\end{aligned}\qquad(A2)$$

where the z-axis is perpendicular to the well interface. A is the interface area of the sample while the δ notation represents momentum conservation within a plane parallel to the well interface. $\phi_{nj}(z_1)$ is the wave function of a carrier which is obtained by the self-consistent solution of the Schrodinger-Poisson equation

for electrons and k.p method for holes. λ_s is the inverse screening length and its relation is as follows [29]

$$\lambda_s^2 = \frac{e^2}{\pi^2\hbar^3\varepsilon_{GaN}}\sum_j\left[m_{cj}f_c(E_{cj})\sqrt{m_{cj}E_{cj}} + m_{vj}f_v(E_{vj})\sqrt{m_{vj}E_{vj}}\right]. \quad (A3)$$

Here m_{cj} and m_{vj} are the effective masses of electrons and holes in the conduction and valance bands, which will be explained in the following. For carrier-longitudinal optical (LO) phonon scattering, the linewidth broadening is obtained by taking the imaginary part of the one-phonon self-energy [30]

$$\Gamma_{njk_\parallel}^{c-ph} = \pi\sum_{k'_\parallel}\sum_{j'}\left|P_n(k_\parallel k'_\parallel, jj')\right|^2 \times\{n_q+1 - f_n(E_{nj'k_\parallel})\}\delta(E_{nj'k'_\parallel}-E+\hbar\omega_{LO}) + \{n_q - f_n(E_{nj'k'_\parallel})\}\delta(E_{nj'k'_\parallel}-E+\hbar\omega_{LO}), \quad (A4)$$

where $\hbar\omega_{LO}=91.13meV^{-1}$ is the energy of the LO phonon and n_q is the phonon number per mode, given by $n_q = 1/[\exp(\beta\hbar\omega_{LO})-1]$. The matrix element P_n for carrier-LO phonon scattering in a two-dimensional QW is given by

$$\left|P_n(k_\parallel k'_\parallel, jj')\right|^2 = \sum_q \frac{e^2\hbar\omega_{LO}}{2V}\left(\frac{1}{\varepsilon_\infty}-\frac{1}{\varepsilon}\right)\frac{q^2}{(q^2+\lambda_s^2)} \times\left|\int \phi_{nj}^*(z)\phi_{nj}(z)\exp(-iq_z)dz\right|^2, \quad (A5)$$

where $\boldsymbol{\varepsilon}_\infty$ is the optical dielectric constants, q_z is the phonon wave vector perpendicular to the well interface and V is the volume of the system. The intraband relaxation time τ_{in} is obtained from Eqs. (A1) and (A4) as $\hbar/\tau_{in} = \Gamma_{cjk_\square}(E)+\Gamma_{vjk_\square}(E)$.

References

[1] C. Boudaoud, A. Hamdoune, Z. Allam, "Simulation and optimization of a tandem solar cell based on InGaN." Mathematics and Computers in Simulation, **167** (2020) 194.

[2] M. Kuc, L. Piskorski, M. Dems, M. Wasiak, A. K. Sokoł, Robert P. Sarzała, T. Czyszanowski, "Numerical Investigation of the Impact of ITO, AlInN, Plasmonic GaN and Top Gold Metalization on Semipolar Green EELs." Materials, **13** (2020) 1444.

[3] A. Tian, L. Hu, L. Zhang, J. Liu, H. Yang, "Design and growth of GaN-based blue and green laser diodes." Science China Materials, **63** (2020) 1348.

[4] A. Pandey, W. J. Shin, J. Gim, R. Hovden, Z. Mi, "High-efficiency AlGaN/GaN/AlGaN tunnel junction ultraviolet light-emitting diodes." Photonics Research, **8** (2020) 331.

[5] X. Huang, H. Chen et al, "Energy band engineering of InGaN/GaN multi-quantum-well solar cells via AlGaN electron- and hole-blocking layers." Applied Physics Letters, **113** (2018) 043501.

[6] A.G. Bhuiyan, K. Sugita, A. Hashimoto, A. Yamamoto, "InGaN solar cells: present state of the art and important challenges," IEEE J Photovoltaics, **2** (2012) 276.

[7] J. Wu, W. Walukiewicz et al., "Small band gap bowing in $In_{1-x}Ga_xN$ alloys." Applied Physics Letters, **80** (2002) 4741.

[8] R. Yahyazadeh, "Effect of hydrostatic Pressure on Optical Absorption Spectrum AlGaN/GaN Multi-quantum wells." Journal of Interfaces, Thin films, and Low dimensional systems, **3** (2021) 279.

[9] R. Yahyazadeh, Z. hashempour, "Effects of Hydrostatic Pressure and Temperature on the AlGaN/GaN High Electron Mobility Transistors." Journal of Interfaces, Thin films, and Low dimensional systems, **2** (2019) 183.

[10] Q. Deng et al., "An investigation on InxGa1−xN/GaN multiple quantum well solar cells," Journal of Physics D: Applied Physice, **44** (2011) 265103.

[11] R. Belghouthi, M. Aillerie, "Temperatur dependece of InGaN/GaN Multiple quantum well solar cell." Energy Procedia, **157** (2019) 793.

[12] B. Chouchen, M. H. Gazzah, A. Bajahzar, Hafedh Belmabrouk, "Numerical Modeling of the Electronic and Electrical Characteristics of InGaN/GaN-MQW Solar Cells." Materials, **12**, (2019) 1241.

[13] R. Yahyazadeh, "Numerical Modeling of the Electronic and Electrical Characteristics of InGaN/GaN Multiple Quantum Well Solar Cells." Journal of Photonics for Energy, **10** (2020) 045504.

[14] X. Huang, "Piezo-Phototronic Effect in a Quantum Well Structure." ACS Nano, **10** (2016) 5145.

[15] O. Ambacher, A. B. Foutz, J. Smart, J. R. Shealy, N. G. Weimann, K. Chu et al., "Two dimensional electron gases induced by spontaneous and piezoelectric polarization in undoped and doped AlGaN/GaN heterostructures." Journal of Applied Physics, **87** (2000) 334.

[16] O. Ambacher, J. Majewski, C. Miskys, et al, "Pyroelectric properties of Al (In) GaN/GaN hetero- and quantum well structures." Journal of Physics Condensed Matter, **14** (2002) 3399.

[17] Z. J. Feng, Z. J. Cheng, and H. Yue, 'Temperature dependence of Hall electron density of GaN-based heterostructures." Chinese Physics **13** (2004) 1334.

[18] V. Fiorentini, F. Bernardini, and O. Ambacher, "Evidence for nonlinear macroscopic polarization in III–V nitride alloy Heterostructures." Applied Physics Letters, **80** (2002) 1204.

[19] P. Perlin, L. Mattos, N. A. Shapiro, J. Kruger, W. S. Wong, T. Sands, N. W. Cheung, E. R. Weber, "Reduction of the energy gap pressure coefficient of GaN due to the constraining presence of the sapphire substrate." Journal of Applied Physics, **85** (1999) 2385.

[20] K. J. Bala, A. J. Peter, C. W. Lee, "Simultaneous effects of pressure and temperature on the optical transition energies in a Ga0.7In0.3N/GaN quantum ring." Chemical Physics, **495** (2017) 42.

[21] I. Vurgaftman, J. R Meyer, L. R. R Mohan, "Band parameters for III–V compound semiconductors and their alloys." Journal of Applied Physics, **8** (2001) 5815.

[22] B. Jogai, "Influence of surface states on the two-dimensional electron gas in AlGaN/GaN heterojunction field-effect transistors." Journal of Applied Physics, **93** (2003) 1631.

[23] B. Jogai, "Parasitic Hole Channels in AlGaN/GaN Heterojunction Structures." Physica status solidi b, **233** (2002) 506.

[24] V. B. Yekta, H. Kaatuzian, "Design considerations to improve high temperature characteristics of 1.3μm AlGaInAs-InP uncooled multiple quantum well lasers: Strain in barriers." Optik. **122** (2011) 514.

[25] J. Piprek. Semiconductor Optoelectronic Devices: Introduction to Physics and Simulation. Elsevier Science, San Diego.California, (2013) 121.

[26] P. S. Zory, Quantum well lasers. Academic San Diego, CA (1993) 58.

[27] C.D. Mahan, Many-body particle physics. Plenum press, New York and London, Chapter 3 (1990).

[28] W. Wei-Ying et al, "Effects of interface roughness on photoluminescence full width at half maximum in GaN/AlGaN quantum wells." Chinese Physics B, **23** (2014) 117803.

[29] R. yahyazadeh, Z. Hashempour. "Numerical Modeling of Electronic and Electrical Characteristics of Multiple Quantum Well Solar Cells $Al_{0.3}Ga_{0.7}N$/GaN." Journal of Optoelectronical Nanostructures, **5** (2020) 81.

[30] S. H. Ha, S. L. Ban, "Binding energies of excitons in a strained wurtzite GaN/AlGaN quantum well influenced by screening and hydrostatic pressure." Journal of Physics Condensed Matter. **20** (2008) 085218.

[31] J.G. Rojas-Briseno, I. Rodriguez-Vargas, M. E. Mora-Ramos, J.C. Martínez-Orozco, "Heavy and light exciton states in c-AlGaN/GaN asymmetric double quantum wells." Physica E, **124** (2020) 114248.

[32] P. Harrison, A. Valavanis, Quantum Wells, Wires and Dots: Theoretical and Computational Physics of Semiconductor Nanostructures, 4th edition, Wiley (2016).

[33] E. Kasapoglu, H. Sari, N. Balkan, I. Sokmen, Y. Ergun, "Binding energy of excitons in symmetric and asymmetric coupled double quantum wells in a uniform magnetic field." Semiconductor Science and Technology, **15** (2000) 219.

[34] J.G. Rojas-Briseño, J.C. Martínez-Orozco, M.E. Mora-Ramos, "States of direct and indirect excitons in strained zinc-blende GaN/InGaN asymmetric quantum wells." Superlattices and Microstructures, **112** (2017) 574.

[35] R Yahyazadeh, Z.Hashempour, "Effect of Hydrostatic Pressure and Temperature on Quantum Confinement of AlGaN/GaN HEMTs." Journal of Science and Technology, **13** (2021) 1.

[36] S.L. Chung, C.S. Chang, "k.p method for strained wurtzite semiconductor." Physical Review B, **54** (1996) 2502.

[37] S. Adachi, Physical Properties of III-V compounds, John Wiley & Sons (1992) 290.

[38] S. R. Chinn, P. S. Zory, A. R. Reisinger, "A Modal for Grin-SCH-SQW Diode Lasers." IEEE Journal of quantum Electronics, **24** (1988) 2191.

[39] I. Tan, G. L. Snider, L. D. Chang, E. L. Hu. "A self-consistent solution of Schrödinger–Poisson equations using a nonuniform mesh." Journal of Applied Physics, **68** (1990) 4071.

[40] X. Huang et al., "Piezo-Phototronic Effect in a Quantum Well Structure." ACS Nano, **10** (2016) 5145.

[41] S. L. Ruminates, M. S. Shur, "Material properties of nitrides summary." International Journal of High Speed Electronics and Systems, **14** (2004) 1.

[42] Chuang, Physics of Photonic Devices, 2nd ed., Wily & Sons (1995).

[43] J. Nelson, "The physics of solar cells." Imperial college press, London (2003)

[44] Z. Dongmei, W. Zongchi, X. Boqi, "Correlated electron–hole transitions in wurtzite GaN quantum dots: the effects of strain and hydrostatic pressure." Journal of Semiconductors, **33** (2012) 052002.